Supplementary Information for

Structural basis of protein substrate processing by human mitochondrial high-temperature requirement A2 protease

This PDF file includes:

Materials and Methods

Protein expression and purification

The codon-optimized *Homo sapiens* S306A HtrA2 gene (residues 134-458 Uniprot: O43464) was synthesized by GenScript and cloned into a pET-SUMO vector as previously described (1, 2). All HtrA2 mutations were introduced by using Quikchange site-directed mutagenesis (Agilent). For producing non-labeled proteins, transformed *E. coli* BL21(DE3) cells were grown in LB media at 37 °C. Cells were induced by adding 0.2 mM isopropyl β-D-1-thiogalactopyranoside (IPTG) at an OD_{600} of ~0.7 and grown for ~18 hours at 25 °C. For producing isotopically-labeled proteins, transformed *E. coli* BL21(DE3) cells were grown in minimal M9 D_2O media supplemented with d_7-glucose as the sole carbon source. For methyl-labeling, the precursors (60 mg/L 2-keto-3-d_2-4-^{13}C-butyrate for Ileδ1-$^{13}CH_3$, 60 mg/L 2-keto-

3,3,4,4-d_4-4-^{13}C-butyrate for Ileδ1-$^{13}CHD_2$, 80 mg/L 2-keto-3-methyl-d_3-3-d_1-4-^{13}C-butyrate for Leu,Val-$^{13}CH_3/^{12}CD_3$ non-stereospecific isopropyl labeling, 230 mg/L 2-hydroxy-2-methyl-d_3-3-oxobutanoate-4-^{13}C for Leuδ1,Valγ1-$^{13}CH_3$, *proR* stereospecific isopropyl labeling, and 100 mg/L methyl-$^{13}CH_3$-methionine for Metε-$^{13}CH_3$) were added 1 hour prior to induction of protein overexpression (3, 4). Cells were induced by adding 0.2 mM IPTG at an OD_{600} of ~0.7 and grown for ~16 hours at 37 °C. Proteins were purified by Ni-affinity chromatography using a 5 mL HisTrap HP column (Cytiva) or HIS-Select Nickel Affinity Gel (Sigma) and eluted in a buffer containing 20 mM HEPES-NaOH (pH 7.4), 300 mM NaCl, 300 mM imidazole. The N-terminal His_6-SUMO tag was cleaved by the addition of Ulp1 protease. Protein purification was further achieved by hydrophobic interaction chromatography with a HiTrap Butyl HP column (Cytiva) using a buffer-gradient of 20 mM HEPES-NaOH (pH 7.4), 0-500 mM $(NH_4)_2SO_4$, 1 mM EDTA. The eluted fractions containing full-length protein were concentrated by using an Amicon Ultra-15 30K MWCO concentrator (Millipore) and subjected to size exclusion chromatography on a Hi-Load 16/600 Superdex 200 pg column or a Superdex 200 Increase column (Cytiva) in a buffer containing 20 mM HEPES-NaOH (pH 7.4), 300 mM NaCl, 1 mM EDTA. Protein concentrations were measured based on molar extinction coefficients at 280 nm (10,430 M^{-1} cm^{-1}). The PDZ-peptide (DDGQYYFV) and the substrate peptide (IRRVSYSF) were synthesized by Genscript. Peptide concentrations were measured based on molar extinction coefficients at 280 nm (2,980 M^{-1} cm^{-1} for the PDZ-peptide and 1,490 M^{-1} cm^{-1} for the substrate peptide). E425C PDZ peptide-stapled HtrA2 proteins were prepared as described previously (2).

The *Drosophila melanogaster* drkN SH3/drkN SH3-PDZbm (residues 1-59 without/with the C-terminal GQYYFV sequence, Uniprot: Q08012) domains were expressed using a construct that incorporates an N-terminal His_6-tag followed by a tobacco etch virus (TEV) protease cleavage site and

purified as described previously (5). The C-terminal PDZ-binding motif or M30C mutation of drkN SH3 was introduced by using Quikchange site-directed mutagenesis (Agilent). For producing unlabeled proteins, transformed *E. coli* BL21(DE3) cells were grown in LB media at 37 °C. Uniformly ^{13}C, ^{15}N-labeled proteins were generated by growing transformed cells in minimal M9 H_2O media supplemented with ^{13}C-glucose and $^{15}NH_4Cl$ as the sole carbon and nitrogen sources, respectively. Uniformly ^{2}H, ^{15}N-labeled proteins were expressed in transformed cells grown in minimal M9 D_2O media supplemented with d_7-glucose and $^{15}NH_4Cl$ as the sole carbon and nitrogen sources, respectively. When ^{13}C-labeling was required, ^{2}H, ^{13}C-glucose was used as the carbon source instead. Methyl-labeling was achieved by growing cells in minimal M9 D_2O media supplemented with d_7-glucose as the sole carbon source along with the addition of precursors (60 mg/L 2-keto-3-d_2-4-^{13}C-butyrate for Ileδ1-$^{13}CH_3$, 80 mg/L 2-keto-3-methyl-d_3-3-d_1-4-^{13}C-butyrate for non-stereospecific Leu,Val-$^{13}CH_3/^{12}CD_3$ labeling of isopropyl methyls, and 100 mg/L methyl-$^{13}CH_3$-methionine for Metε-$^{13}CH_3$) 1 hour prior to induction of protein overexpression (3). Cells were induced by addition of 0.2 mM IPTG at an OD_{600} of ~0.7 and grown for ~18 hours at 25 °C. Proteins were purified by Ni-affinity chromatography on a 5 mL HisTrap HP column (Cytiva) in a buffer containing 50 mM Tris-HCl (pH 8.0), 300 mM NaCl, 6 M guanidinium chloride (GdnCl). The proteins were refolded on the column by gradually reducing the concentration of the denaturing agent in the wash buffer (from 6 M, 3M, 1M, to 0 M GdnCl), and eluted with buffer containing 300 mM imidazole. The N-terminal His_6-tag was removed via TEV protease cleavage. The proteins were further purified by size exclusion chromatography on Hi-Load 16/600 Superdex 75 pg column (Cytiva) in a buffer containing 20 mM Tris-HCl (pH 8.0), 300 mM NaCl, 1 mM EDTA. Protein concentrations were measured based on molar extinction coefficients at 280 nm (8,480 M^{-1} cm^{-1} for drkN SH3 and 11,460 M^{-1} cm^{-1} for drkN SH3-PDZbm).

The trimeric drkN SH3 gene with an N-terminal His_6-SUMO tag and the trimerization domain of T4 bacteriophage fibritin (GYIPEAPRDGQAYVRKDGEWVLLSTFL) (6–9) was synthesized and cloned into a pET-29b vector by Genscript. The C-terminal PDZ-binding motif was introduced by using Quikchange site-directed mutagenesis (Agilent). For producing non-labeled proteins, transformed *E. coli* BL21(DE3) cells were grown in LB media at 37 °C, and cells were induced by adding 1 mM IPTG at an OD_{600} of ~0.8 and grown for 3 hours at 18 °C. Proteins were purified under denaturing conditions using the same protocol as for purification of drkN SH3, described above, except that the N-terminal His_6-SUMO tag was cleaved by Ulp1 protease. Protein concentrations were measured based on the molar extinction coefficient at 280 nm (19,940 M^{-1} cm^{-1}).

The *Gallus gallus* A39V/N53P/V55L Fyn SH3/Fyn SH3-PDZbm (residues 85-142 without/with a C-terminal GQYYFV tag, Uniprot: Q05876) domains were prepared as described previously (10–12). The gene for expression incorporates an N-terminal His_6-tag followed by a TEV protease cleavage site. The C-terminal PDZ-binding motif was introduced by using Quikchange site-directed mutagenesis (Agilent). For producing non-labeled proteins, transformed *E. coli* BL21(DE3) cells were grown in LB media at 37 °C. Cells were induced by addition of 0.2 mM IPTG at an OD_{600} of ~0.7 and grown for ~18 hours at 18 °C. Proteins were purified using the same protocol as for the purification of drkN SH3, described above. Protein concentrations were measured based on the molar extinction coefficients at 280 nm (16,960 M^{-1} cm^{-1} for A39V/N53P/V55L Fyn SH3 and 19,940 M^{-1} cm^{-1} for A39V/N53P/V55L Fyn SH3-PDZbm).

Homo sapiens hTRF1 (residues 378-439 Uniprot: P54274)/hTRF1-PDZbm (residues 378-431, followed by DDGQYYFV) genes were cloned into a pET-SUMO vector by using the Gibson assembly

approach (New England Biolabs). Proteins were prepared as described previously with slight modifications (13, 14). Transformed *E. coli* BL21(DE3) cells were grown in LB media at 37 °C and induced by adding 0.2 mM IPTG at an OD_{600} of ~0.7 and grown for ~18 hours at 18 °C. Proteins were purified by Ni-affinity chromatography on a 5 mL HisTrap HP column (Cytiva) in a buffer containing 50 mM Tris-HCl (pH 8.0), 300 mM NaCl, 6 M GdnCl. The proteins were refolded on the column by gradually reducing the concentration of denaturing agent in the wash buffer (from 6 M, 3M, 1M, to 0 M GdnCl), and eluted with buffer containing 300 mM imidazole. The N-terminal His_6-SUMO tag was cleaved by the addition of Ulp1 protease. Proteins were purified by size exclusion chromatography on a Hi-Load 16/600 Superdex 75 pg column (Cytiva) in a buffer containing 20 mM Tris-HCl (pH 8.0), 300 mM NaCl, 1 mM EDTA, and then further purified by cation exchange chromatography with a Hitrap SP XL 5 mL (Cytiva) column using a gradient of 0 - 1 M NaCl. Protein concentrations were measured based on molar extinction coefficients at 280 nm (24,980 M^{-1} cm^{-1} for hTRF1 and 27,960 M^{-1} cm^{-1} for hTRF1-PDZbm).

Exact amino acid sequences of the SH3 domains and hTRF1 are listed immediately below since they can contain extra amino acids that originate from the TEV protease cleavage site and/or the protein expression vector. The residue numbers for Fyn SH3 and hTRF1 are given according to our previous studies (11, 13).

Amino acid sequence of HtrA2 substrate proteins

Protein	Amino acid sequence
drkN SH3	**G**MEAIAKHDFSATADDELSFRKTQILKILNMEDDSNWYRAELDGKEGLI PSNYIEMKNHD
drkN SH3-PDZbm	**G**MEAIAKHDFSATADDELSFRKTQILKILNMEDDSNWYRAELDGKEGLI PSNYIEMKNHDGQYYFV
Trimeric drkN SH3-PDZbm	GGGGSGYIPEAPRDGQAYVRKDGEWVLLSTFLGGGGSGGGGSGGGGSGG GGSGGGGSGGGGSGGGGSGMEAIAKHDFSATADDELSFRKTQILKILNM EDDSNWYRAELDGKEGLIPSNYIEMKNHDGQYYFV
A39V/N53P/V55L Fyn SH3	**GAMVQIS**TLFEALYDYEARTEDDLSFHKGEKFQILNSSEGDWWEVRSLT TGETGYIPSPYLAPVD**R**
A39V/N53P/V55L Fyn SH3-PDZbm	**GAMVQIS**TLFEALYDYEARTEDDLSFHKGEKFQILNSSEGDWWEVRSLT TGETGYIPSPYLAPVD**R**GQYYFV
hTRF1	RKRQAWLWEEDKNLRSGVRKYGEGNWSKILLHYKFNNRTSVMLKDRWRT MKKLKLISSDSED
hTRF1-PDZbm	RKRQAWLWEEDKNLRSGVRKYGEGNWSKILLHYKFNNRTSVMLKDRWRT MKKLKDDGQYYFV

For drkN SH3 and A39V/N53P/V55L Fyn SH3 domains, amino acids from the tag or the vector sequence are indicated in bold.

^{13}C-MMTS labeling

^{13}C-methyl-methane-thiosulfonate (MMTS) labeling (Figs. 4D-E) of drkN SH3-PDZbm was performed as described previously (15, 16). U-^{2}H, ILV-$^{13}CH_3$, M30C drkN SH3-PDZbm was prepared as described above in the presence of 1 mM DTT. The SH3 domain was buffer-exchanged into a DTT-free buffer by passing the protein solution through a PD-10 desalting column (Cytiva), and subsequently the protein was incubated with 2 equivalents of ^{13}C-MMTS (from 100 mM DMSO stock) at room temperature overnight. Unreacted ^{13}C-MMTS was removed by buffer exchange into NMR buffer (20 mM HEPES-NaOH pD 7.4, 50 mM NaCl, 1 mM EDTA, 100% D_2O).

TEMPO-labeling of HtrA2

Non-labeled V226C/S306A/I441V HtrA2 (Fig. 5D) was prepared as described, in the presence of 1 mM DTT. HtrA2 was buffer-exchanged into a DTT-free buffer by using Amicon Ultra-15 MWCO 30K concentrators (Millipore). Proteins were then incubated with 10 equivalents of 4-maleimido-TEMPO (N-(1-oxyl-2,2,6,6-tetramethyl-4-piperidinyl)maleimide) (Toronto Research Chemicals) and allowed to react overnight at room temperature. Unreacted 4-maleimide-TEMPO was removed by buffer exchange into NMR buffer (20 mM HEPES-NaOH pH 7.4, 50 mM NaCl, 1 mM EDTA, 3% D_2O). The reduced state of the spin-label was prepared by incubating V226C-TEMPO-labeled S306A/I441V HtrA2 with 100 mM L-ascorbic acid overnight, followed by buffer exchange into NMR buffer (20 mM HEPES-NaOH pH 7.4, 50 mM NaCl, 1 mM EDTA, 3% D_2O). We confirmed that ~83% of the available sites were modified with 4-maleimido-TEMPO using electrospray ionization (ESI) mass spectrometry.

SEC-MALS

SEC-MALS experiments (Fig. 3C) were performed using a Superdex 75 HR 10/30 column (Pharmacia) and Infinity-II HPLC (Agilent) system connected to MiniDAWN TREOS MALS and OptiLab T-rEX refractive index components (Wyatt Technology). A buffer containing 20 mM Tris-HCl (pH 8.0) and 150 mM NaCl was used. Prior to the analyses, the system was calibrated using bovine serum albumin as a standard. 100 μL of a sample containing 50 μM drkN SH3-PDZbm or 50 μM trimeric drkN SH3-PDZbm (as a monomer) was injected. The data were analyzed with ASTRA software (Wyatt Technology).

Proteolysis assay

The proteolytic activity of HtrA2 was measured by incubating 50 μM of the substrate protein with 10 μM wild-type HtrA2 at 37 °C for 2 hrs in a buffer containing 20 mM Tris-HCl (pH 8.0), 150 mM NaCl, and 1 mM EDTA (Fig. 1D and *SI Appendix* Fig. S1). Control reactions were also performed by incubating substrate protein without adding HtrA2. For measuring the time course of the cleavage reactions, 20 μM of the substrate protein was incubated with 2 μM wild-type HtrA2 at 37 °C (Figs. 3D-E). At each time point, an aliquot of the reaction solution was collected and the reaction was quenched by mixing with lithium dodecyl sulfate (LDS) sample buffer followed by heating at 95 °C for 3 mins. The samples were analyzed by SDS-PAGE using NuPAGE™ 4 to 12%, Bis-Tris Gels (Thermo Fisher Scientific). The band intensities of the intact proteins were quantified by using the software ImageJ 1.52a (17).

For identifying the cleavage site(s) of drkN SH3-PDZbm, 30 μM drkN SH3-PDZbm was incubated with 5 μM HtrA2 at 37 °C for 15 hrs in a buffer containing 20 mM HEPES-NaOH (pH 7.4) and 1 mM EDTA, and the mass of the components from the reaction mixture was determined using mass spectrometry by first separating them via high-performance liquid chromatography (HPLC). Determination of the peptide fragments in the reaction mixture was performed at the AIMS Mass Spectrometry Facility, Department of Chemistry, University of Toronto. ESI mass spectra were acquired using a 6538 UHD model quadrupole time-of-flight mass spectrometer equipped with a 1260 Infinity Series HPLC (Agilent). The fragments were assigned using FindPept software tool (https://web.expasy.org/findpept/) (*SI Appendix* Supplementary Table 1) (18).

NMR experiments

All NMR measurements were performed at 23.5 Tesla (1 GHz ^{1}H frequency) on a Bruker Avance Neo spectrometer, 18.8 Tesla (800 MHz ^{1}H frequency) or 14.0 T (600 MHz ^{1}H frequency) on Bruker Avance III HD spectrometers, all equipped with cryogenically cooled *x*, *y*, *z* pulsed-field gradient triple-resonance probes. All spectra were processed and analyzed using the *NMRPipe* suite of programs (19) and visualized using the Python package *nmrglue* (20). 3D datasets were recorded with non-uniform-sampled time-domain data based on Poisson-Gap sampling schedules (21), and the spectra were reconstructed using SMILE (22). Peak intensities were extracted either by using the Peakipy software package (https://github.com/j-brady/peakipy), *PINT* software (23, 24), or by ellipsoidal sum integration using an in-house Python script. The methyl signal assignments were transferred from previous studies (1, 25).

Titrations of U-^{2}H, ^{15}N drkN SH3-PDZbm into solutions of U-^{2}H, *proR* ILVM-labeled S306A/I441V HtrA2 (Fig. 2 and *SI Appendix*, Fig. S2A) or U-^{2}H, *proR* ILVM-labeled E425C/S306A/I441V PDZ peptide-stapled S306A/I441V HtrA2 (*SI Appendix*, Fig. S3) were performed at 40 °C, in an NMR buffer consisting of 20 mM HEPES-NaOH (pD 7.4), 50 mM NaCl, 1 mM EDTA, 100% D_2O. The concentrations of U-^{2}H, ^{15}N drkN SH3-PDZbm used in the titration of U-^{2}H, *proR* ILVM-labeled S306A/I441V HtrA2 were 0, 34, 71, 111, 148, 193, 244, 297, 342, 419, and 490 μM and 0, 72, 160, 251, 362, 503, 704, 864 μM for the titration involving U-^{2}H, *proR* ILVM-labeled E425C/S306A/I441V PDZ peptide-stapled HtrA2. Reference spectra (Fig. 2A) of the closed and open inactive HtrA2 states were obtained using a 150 μM (monomer concentration) U-^{2}H, ILVM-labeled S306A/I441V HtrA2 sample without and with 1 mM PDZ-peptide, respectively, in an NMR buffer consisting of 20 mM HEPES-NaOH (pD 7.4), 1 mM EDTA, 100% D_2O. The reference spectrum for the

open active state of HtrA2 (Fig. 2A) was obtained using a 100 μM (monomer concentration) U-^{2}H, *proR* ILVM-labeled S306A/I441V HtrA2 sample with 1 mM PDZ-peptide and 2 mM substrate peptide in an NMR buffer consisting of 20 mM HEPES-NaOH (pD 7.4), 200 mM NaCl, 1 mM EDTA, 100% D_2O. ^{13}C-^{1}H HMQC spectra that exploit the methyl-TROSY effect were recorded as described previously (26, 27).

2D ^{13}C[t_1]-t_{mix}-^{1}H[t_2] and 3D ^{1}H[t_1]-^{13}C[t_2]-t_{mix}-^{1}H[t_3] ZZ-exchange experiments to correlate closed and open inactive states (*SI Appendix*, Fig. S2B) were measured at a static magnetic field strength of 23.5 Tesla and 40 °C, using a 160 μM (monomer concentration) U-^{2}H, *proR* ILVM-labeled S306A HtrA2 sample with 100 μM U-^{2}H PDZ-peptide in an NMR buffer consisting of 20 mM HEPES-NaOH (pD 7.4), 1 mM EDTA, 100% D_2O, as described previously (1). The mixing time was set to 50 ms. 2D ^{13}C[t_1]-t_{mix}-^{1}H[t_2] magnetization exchange experiments to correlate open inactive and open active states (*SI Appendix*, Fig. S2C) were measured at a static magnetic field strength of 14.0 Tesla and 50 °C, as described previously (2). A 200 μM (monomer concentration) U-^{2}H, Ile-$^{13}CHD_2$ S306A/I441V HtrA2 sample containing 4 mM PDZ-peptide was used. The mixing time was set to 900 ms.

2D ^{13}C-^{1}H HMQC (Fig. 4A) and 2D ^{13}C[t_1]-t_{mix}-^{1}H[t_2] ZZ-exchange (*SI Appendix*, Fig. S5) experiments were recorded on solutions of 150 μM U-^{2}H, ILVM-labeled drkN SH3-PDZbm with 0, 75, or 150 μM U-^{2}H S306A/I441V HtrA2 in an NMR buffer consisting of 20 mM HEPES-NaOH (pD 7.4), 50 mM NaCl, 1 mM EDTA, 100% D_2O (23.5 Tesla and 40 °C). For ZZ-exchange experiments, mixing times ranging from 2 to 200 ms were used (*SI Appendix*, Fig. S5).

^{13}C single quantum Carr-Purcell-Meiboom-Gill (CPMG) relaxation dispersion experiments were recorded on 150 μM U-^{2}H, ILVM-labeled drkN SH3-PDZbm samples with or without 150 μM (monomer concentration) U-^{2}H S306A/I441V HtrA2 in an NMR buffer consisting of 20 mM HEPES-NaOH (pD

7.4), 50 mM NaCl, 1 mM EDTA, 100% D_2O either at 40 °C (Fig. 4B) or at 10 °C (*SI Appendix,* Fig. S6A). In order to ensure that binding to HtrA2 was responsible for the elevated relaxation rates, a control experiment was performed at 40°C using a sample comprising 150 μM U-^{2}H, ILVM-labeled drkN SH3 (no C-terminal PDZ-binding motif) and 150 μM (monomer concentration) U-^{2}H S306A/I441V HtrA2 in an NMR buffer consisting of 20 mM HEPES-NaOH (pD 7.4), 50 mM NaCl, 1 mM EDTA, 100% D_2O (*SI Appendix* Fig. S6B). Note that in the absence of the PDZ-binding motif the interaction between drkN SH3 and HtrA2 is very weak. A pulse scheme described previously (28) was employed at a static magnetic field of 23.5 Tesla. Two CPMG fields of 50 Hz and 2 kHz were used with a constant-time relaxation delay of 25 ms (*SI Appendix,* Fig. S6A) or 40 ms (Fig. 4B, *SI Appendix* Fig. S6B).

$S^2_{\text{axis}}\tau_c$ values of drkN SH3 side-chain methyl groups were recorded using 150 μM U-^{2}H, ILVM-labeled drkN SH3-PDZbm samples with or without 150 μM (monomer) U-^{2}H S306A/I441V HtrA2 in an NMR buffer consisting of 20 mM HEPES-NaOH (pD 7.4), 50 mM NaCl, 1 mM EDTA, 100% D_2O (Fig. 4C). A control experiment was performed using a sample with 150 μM U-^{2}H, ILVM-labeled drkN SH3 (without the PDZ-binding motif) + 150 μM (monomer) U-^{2}H S306A/I441V HtrA2 in an NMR buffer consisting of 20 mM HEPES-NaOH (pD 7.4), 50 mM NaCl, 1 mM EDTA, 100% D_2O. (*SI Appendix* Fig. S6C). Values were measured by monitoring the build-up of the methyl ^{1}H triple quantum coherence as previously described (1, 29) at a static magnetic field of 23.5 Tesla and 10 °C. Relaxation delays ranging from 2.5-50 ms were used.

2D, ^{13}C-edited ^{1}H[t_1]-t_{mix}-^{1}H[t_2] ZZ-exchange experiments (30) of U-^{2}H, ILV-$^{13}CH_3$, M30C ^{13}C-MMTS-labeled drkN SH3-PDZbm were recorded at a static magnetic field strength of 23.5 Tesla and 40 °C (Fig. 4D), using a sample containing 150 μM U-^{2}H, ILV-$^{13}CH_3$, M30C ^{13}C-MMTS-labeled drkN

SH3-PDZbm + 75 μM U-^{2}H S306A/I441V HtrA2 in an NMR buffer consisting of 20 mM HEPES-NaOH (pD 7.4), 50 mM NaCl, 1 mM EDTA, 100% D_2O. In this experiment exchange of longitudinal order, H_ZC_Z, where *H* and *C* are carbon and proton spins, respectively, is quantified, with a total of 14 mixing times ranging from 1 to 250 ms.

3D HNCO spectra of U-^{15}N, ^{13}C drkN SH3 were recorded at a static magnetic field strength of 14.0 Tesla and 10 °C, using 300 μM U-^{15}N, ^{13}C drkN SH3 samples with 0, 60, or 100 μM (monomer concentration) unlabeled S306A/I441V HtrA2 in an NMR buffer consisting of 20 mM HEPES-NaOH (pH 7.4), 50 mM NaCl, 1 mM EDTA, 1 mM PDZ-peptide, 3% D_2O (Fig. 5B). Sequential backbone resonance assignments of drkN SH3 were obtained using standard triple-resonance experiments including HNCACB, HBCBCACONNH, and HNN (31, 32).

Transferred cross-saturation (TCS) experiments (33–35) were recorded at a static magnetic field strength of 14.0 Tesla and 10 °C, using 300 μM U-^{2}H, ^{15}N, ^{13}C drkN SH3 samples with or without 150 μM (monomer concentration) unlabeled S306A/I441V HtrA2 in a buffer consisting of 20 mM HEPES-NaOH (pH 7.4), 50 mM NaCl, 1 mM EDTA, 1 mM PDZ-peptide, 80% D_2O (Fig. 5C, *SI Appendix*, Fig. S7). 3D TROSY-HNCO spectra (36, 37) were recorded with or without 2 sec ^{1}H WURST adiabatic decoupling (38) centered on 1 ppm with a bandwidth of 2 ppm. The TCS effects were quantified from the signal intensity ratio with and without the ^{1}H radio frequency irradiation.

PREs plotted in Figure 5D were directly calculated from differences in ^{1}H linewidths measured in HNCO spectra recorded on paramagnetic and diamagnetic samples by 3D peak-shape fitting using PINT (23, 24). Datasets were processed with an exponential line-broadening window function (5 Hz) in the direct ^{1}H dimension. The samples contained 240 μM U-^{15}N, ^{13}C drkN SH3 and 120 μM (monomer

concentration) V226C-TEMPO-labeled S306A/I441V HtrA2 (either oxidized or reduced) in an NMR buffer consisting of 20 mM HEPES-NaOH (pH 7.4), 50 mM NaCl, 1 mM EDTA, 1 mM PDZ-peptide, 3% D_2O.

Fitting of NMR titration data (Fig. 2D, SI Appendix Fig. S3B)

As described in the main text, drkN SH3-PDZbm titration profiles (Figs. 2B, C) were fit to a model that assumes stepwise binding of drkN SH3-PDZbm to HtrA2, with positive cooperativity. During the course of the titration HtrA2 converts from a closed conformation (C) to open inactive (OI) and finally open active (OI) states (Fig. 2D). This model was motivated by our previous binding studies using peptide ligands where the C to OI and OI to OA transitions could be separated, as each process is triggered by separate peptides (1, 2). In what follows, we denote an HtrA2 trimer as P_3, the drkN SH3-PDZbm ligand as L, and each ligand-bound form of P_3 as P_3L_j, where j is the number of drkN SH3-PDZbm molecules tethered to the HtrA2 trimer via interactions involving PDZ domains and PDZ-binding motifs of HtrA2 and ligand, respectively. We performed two different titration experiments: (*i*) drkN SH3-PDZbm titration to a solution of the native HtrA2 trimer to characterize the complete substrate binding pathway (Figs. 2B, 2C, *SI Appendix,* Fig. S2A) and (*ii*) titration of drkN SH3-PDZbm to E425C PDZ peptide-stapled open HtrA2 trimer (2) to selectively characterize the binding of untethered drkN SH3-PDZbm to the OI state of HtrA2 (*SI Appendix*, Fig. S3A). The association constant of the untethered drkN SH3-PDZbm domain to the protease domain of HtrA2, obtained from titration (*ii*), was used in the analysis of the profiles generated from titration (*i*) to get robust estimates of the association constants for each step of the binding reaction (see main text).

(*i*) Fitting of drkN SH3-PDZbm titration profiles using methyl probes from native HtrA2 (Fig. 2D)

As described in the main text, binding of drkN SH3-PDZbm to HtrA2 is assumed to proceed via the following thermodynamic model (Fig. 2D)

$$\begin{aligned} P_3 + L \rightleftarrows P_3L \qquad & 3K_1 = \frac{[P_3L]}{[P_3][L]} \\ P_3L + L \rightleftarrows P_3L_2 \qquad & \alpha K_1 = \frac{[P_3L_2]}{[P_3L][L]} \\ P_3L_2 + L \rightleftarrows P_3L_3 \qquad & \frac{1}{3}\alpha^2 K_1 = \frac{[P_3L_3]}{[P_3L_2][L]} \end{aligned} \qquad [1]$$

$$\begin{aligned} P_3L_3 \rightleftarrows P_3^*L_3 \qquad & K_2 = \frac{[P_3^*L_3]}{[P_3L_3]} \\ P_3L_3 + L \rightleftarrows P_3^*L_4 \qquad & K_3 = \frac{[P_3^*L_4]}{[P_3L_3][L]} \end{aligned}$$

which includes free (P_3), partially-ligated (P_3L and P_3L_2, where one or two ligand-molecules are tethered to a trimer), and fully-ligated (P_3L_3) trimeric states. As illustrated schematically in Figure 2D, binding occurs at the level of interactions between the PDZ domains of HtrA2 and the PDZ binding motifs attached to the C-termini of drkN SH3, but may also include the second prong of the interaction that involves substrate, protease domain contacts (Fig. 2D). In addition, two distinct catalytically active states, $P^*_3L_3$ and $P^*_3L_4$ (asterisk denotes the OA state), are included, where the drkN SH3-PDZbm substrates (either PDZ-bound or untethered) form contacts with the protease domains of HtrA2. K_1 is the *microscopic* association constant for binding of drkN SH3-PDZbm to a PDZ domain of HtrA2, and the factors of 3 and 1/3 take into account the three ways in which one molecule of L can either bind to P_3 or be removed from P_3L_3. K_2 is the unimolecular equilibrium constant for the interconversion between the fully PDZ-bound OI state (P_3L_3) and the OA state ($P^*_3L_3$), and K_3 is the macroscopic association constant for the binding of an untethered drkN SH3-PDZbm molecule (*i.e.*, not attached to HtrA2) to an exposed protease domain

of HtrA2, forming the OA state. To account for the positive cooperativity of the binding of ligand (1, 2), a single cooperativity factor α was introduced. Note that no assumption is made as to the number of protease-bound drkN SH3-PDZbm molecules in the OA states, ($P^*_3L_3$, $P^*_3L_4$), as this information is not available from this titration. The transition from OI to OA is described most simply, therefore, by the pair of macroscopic constants K_2 and K_3, and must include formation of one or more contacts between ligands and active sites, as this is required for an OA conformation (2). As described in *Discussion* in the main text, a combined analysis that includes magnetization exchange experiments focusing on the ligand (Fig. 4) does strongly imply that the majority of protease active sites are occupied in the active state, and very likely some in P_3L_3.

The total HtrA2 protomer (C_T) and drkN SH3-PDZbm (L_T) concentrations are defined as follows.

$$\begin{aligned} C_T &= 3[P_3] + 3[P_3L] + 3[P_3L_2] + 3[P_3L_3] + 3[P_3^*L_3] + 3[P_3^*L_4] \\ L_T &= [L] + [P_3L] + 2[P_3L_2] + 3[P_3L_3] + 3[P_3^*L_3] + 4[P_3^*L_4] \end{aligned} \quad [2]$$

with C_T = 150 μM and L_T varied from 0 to 490 μM. The relative intensities of each of states C, OI and OA change during the course of the titration, with their fractional populations given as p_i ($i \in \{\text{C, OI, OA}\}$) with

$$\begin{aligned} p_C &= \frac{(3[P_3] + 2[P_3L] + [P_3L_2])}{C_T} \\ p_{OI} &= \frac{([P_3L] + 2[P_3L_2] + 3[P_3L_3])}{C_T} \\ p_{OA} &= \frac{(3[P_3L_3^*] + 3[P_3L_4^*])}{C_T} \end{aligned} \quad [3]$$

Thus, if the total signal intensity for methyl j is I^0_j (sum of the signal intensities from all three states) then

the signal contribution from state *i* to this maximum intensity is simply $p_i \times I^0_j$.

A number of assumptions have been made in fits of the above model to our titration data based on our previous results using short PDZ-binding and substrate peptides (1, 2). First, as described in the main text, we assume that the unbound protomers in each P_3L_j ($j \in \{0 \text{ to } 3\}$) state contribute to C state signal intensities in an amount proportional to $\sum_{j=0}^{2}(3-j)[P_3L_j]$, while the bound protomers contribute to OI signals according to $\sum_{j=1}^{3} j[P_3L_j]$. Further, all of the protomers in $P^*_3L_3$ and $P^*_3L_4$ contribute equally to OA state signal intensities, reflecting a highly cooperative structural transition from OI to OA, that is consistent with experiments reported previously (2). Second, we assumed that formation of the OA state occurs solely through the fully PDZ-occupied state (P_3L_3), so that formation of the OA conformation cannot occur when only one or two drkN SH3-PDZbm domains are bound (*i.e.*, P^*_3L and $P^*_3L_2$ do not exist). Third, we limited the number of bound drkN SH3-PDZbm molecules to 4 ($P^*_3L_4$; *i.e.*, only a single non-tethered substrate) as it is likely that, in the P_3L_3 state, each substrate-binding site on the protease domains of two HtrA2 protomers are occupied by PDZ-tethered drkN SH3-PDZbm, with only one remaining site, on the protease domain of the third protomer, available for binding an extra drkN SH3-PDZbm substrate (see *Discussion* in the main text for details). Fourth, we fixed the degree of positive cooperativity to be the same for the second and third binding events (represented by the single cooperativity factor α), motivated by the fact that the cooperativity factors for these steps were similar in the case of binding of the PDZ-peptide to HtrA2 (1). Further, we defined α according to the relation, $\alpha = \sqrt{\frac{K_{3rd}}{K_{2nd}} \times \frac{K_{2nd}}{K_{1st}}}$, where K_{1st}, K_{2nd}, and K_{3rd} are the microscopic binding affinities for the 1st, 2nd, and 3rd binding reactions obtained in a previous study using the PDZ-peptide (1).

During the fitting procedure signal losses caused by transverse ^{1}H relaxation during a pair of

magnetization transfer elements in the ^{13}C-^{1}H HMQC pulse sequence were corrected as in Eq. [4] where $R_{i,j}$ is the ^{1}H transverse relaxation rate for methyl *j* in state *i* and τ is the net magnetization transfer time that must be accounted for (= 7.2 ms). The ^{1}H relaxation rates were directly evaluated from ^{1}H linewidths in ^{13}C-^{1}H HMQC datasets (L_T = 0 for measurement of rates for state C or 490 μM to obtain rates for OI and OA) processed with an exponential line-broadening window function (5 Hz). Taking these into account, the NMR signal intensities, $I_{i,j}$, were calculated as

$$I_{i,j} = I_j^0 \times \exp(-R_{i,j}\tau) \times p_i \qquad [4]$$

where *i* is a conformational state (C, OI, and OA) and *j* is the index of a methyl probe used in the fitting. In the analysis of the titration profiles signals of the methyl groups from I150, I274, I362, L377, and M420 were used. These residues were chosen because peaks reporting on at least one of the three states were well resolved so that accurate estimates of peak volumes could be obtained. Due to the limited resolution, signals from two conformational states were overlapped in many cases. For these overlapping residues, the sums of intensities were used for fits as indicated in the Table below.

List of the methyl correlations used in the fitting

Residue	Conformational states	Fractional populations	^{1}H R_2 rates used to correct intensities (Eq. [4])
I150	C + OI	$p_C + p_{OI}$	$R_{2,C}$ = 32.4 s^{-1}, $R_{2,OI}$ = 134.0 s^{-1}
	OA	p_{OA}	$R_{2,OA}$ = 69.5 s^{-1}
I274	C	p_C	$R_{2,C}$ = 42.5 s^{-1}
	OA	p_{OA}	$R_{2,OA}$ = 89.7 s^{-1}
I362	OI + OA	$p_{OI} + p_{OA}$	$R_{2,OI} = R_{2,OA}$ = 73.7 s^{-1}
L377	C	p_C	$R_{2,C}$ = 73.1 s^{-1}
	OI + OA	$p_{OI} + p_{OA}$	$R_{2,OI} = R_{2,OA}$ = 55.5 s^{-1}
M420	C	p_C	$R_{2,C}$ = 28.7 s^{-}
	OI + OA	$p_{OI} + p_{OA}$	$R_{2,OI} = R_{2,OA}$ = 27.1 s^{-1}

Peaks from I274 in the OI state and I362 in the C state were excluded from the analysis because of severe broadening and signal overlap.

The association constant K_1, the unimolecular equilibrium constant K_2, and residue-specific maximum signal intensities I^0_j ($j \in$ I150, I274, I362, L377, M420) were treated as fitted parameters. The cooperativity factor α was fixed to 2.1, as described above, consistent with our previous PDZ-peptide titration results (1), and the association constant K_3 was fixed to 5,470 M^{-1}, obtained from a separate titration using PDZ peptide-stapled HtrA2 (that is in the open conformation (2)) as described in subsection (*ii*) below. Optimal association constants were obtained using a nested minimization procedure as described previously (1). In the first minimization, C_T and L_T values along with initial association constant estimates were passed into Python 3.7's SciPy 1.3 library root-finding algorithm *scipy.optimize.root* to determine the free and ligand-bound protein concentrations. This is achieved by solving systems of

equations relating protein concentrations to equilibrium constants and C_T and L_T values, as per Eqs. [1] and [2], above. In the second minimization step, the extracted concentrations were used to compute fractional populations for the three states (C, OI, and OA) (Eq. [3]) and NMR signal intensities for each titration point were calculated using Eq. [4]. The optimal values of K_1, K_2, and the residue-specific maximum signal intensities I^0_j were obtained by minimizing the residual sum-of-squared (RSS) differences between experimental and calculated signal intensities according to

$$RSS = \sum_i \sum_j \sum_{k=1}^{N} \left(I_{i,j}^{exp.}(L_{T,k}) - I_{i,j}^{calc.}(L_{T,k}, I_j^0, K_1, K_2) \right)^2 \qquad [5]$$

where $I_{i,j}^{exp.}(L_{T,k})$ and $I_{i,j}^{calc.}(L_{T,k}, I_j^0, K_1, K_2)$ ($i \in$ {C, OI, OA}, $j \in$ {I150, I274, I362, L377, M420}) are the experimental and calculated intensities, respectively, and N is the total number of titration points. Minimization of the above target function was achieved using in-house written programs (Python 3.7), exploiting the Levenberg-Marquardt algorithm of the Lmfit python software package (https://lmfit.github.io/lmfit-py/). Distributions of fitted parameters were obtained by running 500 Monte-Carlo simulations, and fitted parameter errors were taken as the standard deviations of these parameter sets. Fitting to the different models as shown in *SI Appendix*, Fig. S4 was performed by setting $K_3 = 0$ (*SI Appendix*, Fig. S4B) or $K_2 = 0$ (*SI Appendix*, Fig. S4C).

(*ii*) Fitting drkN SH3-PDZbm titration profiles using methyl probes from PDZ peptide-stapled HtrA2 (*SI Appendix*, Fig. S3B)

To obtain K_3, the association constant for binding of drkN SH3-PDZbm to the protease domain of HtrA2, we performed a titration of U-^{2}H, ^{15}N drkN SH3-PDZbm and U-^{2}H, *proR* ILVM-labeled

E425C/S306A/I441V PDZ peptide-stapled HtrA2, in which the PDZ-peptide is covalently attached to all of the PDZ domains of HtrA2 to form a constitutively open HtrA2 conformation (2). The thermodynamic model describing the binding scheme is

$$\begin{aligned} P_3' + L &\rightleftarrows P_3'L & 3K &= \frac{[P_3'L]}{[P_3'][L]} \\ P_3'L + L &\rightleftarrows P_3'L_2 & K &= \frac{[P_3'L_2]}{[P_3'L][L]} \\ P_3'L_2 + L &\rightleftarrows P_3'L_3 & \frac{1}{3}K &= \frac{[P_3'L_3]}{[P_3'L_2][L]} \end{aligned} \qquad [6]$$

where P'_3 is PDZ peptide-stapled HtrA2 and L denotes drkN SH3-PDZbm. Note that binding can only occur to the protease domains of HtrA2, as the PDZ domains are saturated with PDZ-peptide (that is covalently attached). We have assumed that the formation of the OA state requires binding of drkN SH3-PDZbm ligands to the three protease domains of a given HtrA2 trimer, as the formation of the OA state is a highly-cooperative process that involves structural transitions of all three protease domains in a trimer (2), and that the macroscopic affinity for the 3rd binding step (= K/3) in the above model is equal to K_3 in the model describing titration (*i*), above. (Note that our data are consistent with two of the three protease domains in P_3L_3 bound with substrate so that the transition from P_3L_3 to P_3L_3* involves binding to one additional protease domain, essentially step 3 in Eq. [6] above). The total HtrA2 protomer concentration (C_T) and drkN SH3-PDZbm ligand (L_T) concentrations are defined as follows,

$$\begin{aligned} C_T &= 3[P_3'] + 3[P_3'L] + 3[P_3'L_2] + 3[P_3'L_3] \\ L_T &= [L] + [P_3'L] + 2[P_3'L_2] + 3[P_3'L_3] \end{aligned} \qquad [7]$$

where C_T = 100 μM and L_T was varied from 0 to 860 μM. The NMR signal intensities of methyl groups

from the OI and OA conformers (I_{OI} and I_{OA}) were calculated as

$$I_{OI} = I^0_{OI} \times \frac{3[P'_3] + 3[P'_3L] + 3[P'_3L_2]}{C_T}$$
$$I_{OA} = I^0_{OA} \times \frac{3[P'_3L_3]}{C_T} \qquad [8]$$

where I^0_{OI} and I^0_{OA} are the intensities at zero ligand and infinite ligand concentrations, respectively, neglecting transverse relaxation (transverse relaxation will only modify I^0_{OI}, I^0_{OA} with no influence on the extracted *K* value). To obtain *K*, peak volumes from methyl groups I150 and I274, reporting on the OI and the OA states were used in the fitting. In addition to *K*, $I^0_{i,j}$ values, $i \in$ {OI, OA}, $j \in$ {I150, I274} were treated as fitting parameters. The optimal *K* and $I^0_{i,j}$ values were obtained by minimizing the RSS differences according to

$$RSS = \sum_i \sum_j \sum_{k=1}^{N} \left(I^{exp.}_{i,j}(L_{T,k}) - I^{calc.}_{i,j}(L_{T,k}, I^0_{i,j}, K) \right)^2 \qquad [9]$$

where $I^{exp.}_{i,j}(L_{T,k})$ and $I^{calc.}_{i,j}(L_{T,k}, I^0_{i,j}, K)$ ($i \in$ {OI, OA}, $j \in$ {I150, I274}) are the experimental and calculated NMR signal intensities at each ligand concentration ($L_{T,k}$), and *N* is the total number of titration points. Minimization of the above target function was achieved using in-house written programs (Python 3.7), exploiting the Levenberg-Marquardt algorithm of the Lmfit python software package (https://lmfit.github.io/lmfit-py/). Distributions of fitted parameters were obtained by running 500 Monte-Carlo simulations, and fitted parameter errors were taken as the standard deviations of these parameter sets.

Fitting magnetization exchange (Fig. 4E)

Magnetization exchange data quantifying the kinetics of association of drkN SH3-PDZbm and HtrA2 were recorded on a sample of 150 μM U-^{2}H, ILV-$^{13}CH_3$, M30C ^{13}C-MMTS-labeled drkN SH3-PDZbm (NMR visible) + 75 μM U-^{2}H S306A/I441V HtrA2 (NMR invisible). The resulting time profiles were fit to a triangular exchange scheme to extract transition rate constants (Fig. 4E), as described previously (5). The kinetic model includes folded (*F*), unfolded (*U*), and bound (*B*) states (Fig. 4F). The evolution of magnetization during the mixing period was calculated using the following matrix differential equation,

$$\frac{d}{dt}\vec{M} = (\vec{K} - \vec{R})\vec{M}$$

$$\vec{M} = \begin{bmatrix} M_F \\ M_U \\ M_B \end{bmatrix}$$

$$\vec{K} = \begin{bmatrix} -k_{FU} - k_{FB} & k_{UF} & k_{BF} \\ k_{FU} & -k_{UF} - k_{UB} & k_{BU} \\ k_{FB} & k_{UB} & -k_{BF} - k_{BU} \end{bmatrix} \qquad [10]$$

$$\vec{R} = \begin{bmatrix} R_F & 0 & 0 \\ 0 & R_U & 0 \\ 0 & 0 & R_B \end{bmatrix}$$

where k_{ij} ($i, j \in$ {F, U, B}) is the transition rate constant from the state *i* to *j*, and R_i ($i \in$ {F, U, B}) are effective relaxation rates during the mixing period. The rate constants are required to satisfy the relationship $k_{FU}k_{UB}k_{BF} = k_{FB}k_{BU}k_{UF}$, ensuring microscopic reversibility. Diagonal- and cross-

peak intensities can be obtained by solving Eq. [10]. The intensities of diagonal-peaks are given by

$$
\begin{aligned}
I_F^{calc.}(t) &= c\,[1 \quad 0 \quad 0] exp\{(\vec{K}-\vec{R})t)\} \begin{bmatrix} M_F^{eq.} \\ 0 \\ 0 \end{bmatrix} \\
I_U^{calc.}(t) &= c\,[0 \quad 1 \quad 0] exp\{(\vec{K}-\vec{R})t)\} \begin{bmatrix} 0 \\ M_U^{eq.} \\ 0 \end{bmatrix} \\
I_B^{calc.}(t) &= c\,[0 \quad 0 \quad 1] exp\{(\vec{K}-\vec{R})t)\} \begin{bmatrix} 0 \\ 0 \\ M_B^{eq.} \end{bmatrix}
\end{aligned}
\qquad [11]
$$

and those of cross-peaks are given by

$$
\begin{aligned}
I_{FU}^{calc.}(t) = I_{UF}^{calc.}(t) &= c\,[1 \quad 0 \quad 0] exp\{(\vec{K}-\vec{R})t)\} \begin{bmatrix} 0 \\ M_U^{eq.} \\ 0 \end{bmatrix} \\
&= c\,[0 \quad 1 \quad 0] exp\{(\vec{K}-\vec{R})t)\} \begin{bmatrix} M_F^{eq.} \\ 0 \\ 0 \end{bmatrix} \\
I_{FB}^{calc.}(t) = I_{BF}^{calc.}(t) &= c\,[1 \quad 0 \quad 0] exp\{(\vec{K}-\vec{R})t)\} \begin{bmatrix} 0 \\ 0 \\ M_B^{eq.} \end{bmatrix} \\
&= c\,[0 \quad 0 \quad 1] exp\{(\vec{K}-\vec{R})t)\} \begin{bmatrix} M_F^{eq.} \\ 0 \\ 0 \end{bmatrix} \\
I_{UB}^{calc.}(t) = I_{BU}^{calc.}(t) &= c\,[0 \quad 1 \quad 0] exp\{(\vec{K}-\vec{R})t)\} \begin{bmatrix} 0 \\ 0 \\ M_B^{eq.} \end{bmatrix} \\
&= c\,[0 \quad 0 \quad 1] exp\{(\vec{K}-\vec{R})t)\} \begin{bmatrix} 0 \\ M_U^{eq.} \\ 0 \end{bmatrix}
\end{aligned}
\qquad [12]
$$

where $I_i^{calc.}(t)$ ($i \in$ {F, U, B}) are diagonal-peak signal intensities at time *t*, $I_{ij}^{calc.}(t)$ ($i, j \in$ {F, U, B})

are cross-peak intensities of correlations whose resonance frequencies in the F_1 and F_2 dimensions derive from the *i* and *j* states respectively, *c* is a global constant of proportionality that converts magnetization to peak volume, and $M_i^{eq.}$($i \in$ {F, U, B}) denotes the magnetization of state *i* immediately prior to the start of the mixing period, which we have assumed is equal to the equilibrium magnetization of that state. $M_i^{eq.}$ is related to fractional populations p_i ($i \in$ {F, U, B}) that, in turn, are functions of the rate constants as follows,

$$\begin{aligned} M_F^{eq.} &= M^{tot.} \times p_F \; ; \;\; p_F = \frac{k_{BF}k_{UF}}{(k_{FB}k_{UF} + k_{BF}k_{UF} + k_{BF}k_{FU})} \\ M_U^{eq.} &= M^{tot.} \times p_U \; ; \;\; p_U = \frac{k_{BF}k_{FU}}{(k_{FB}k_{UF} + k_{BF}k_{UF} + k_{BF}k_{FU})} \\ M_B^{eq.} &= M^{tot.} \times p_B \; ; \;\; p_B = \frac{k_{FB}k_{UF}}{(k_{FB}k_{UF} + k_{BF}k_{UF} + k_{BF}k_{FU})} \end{aligned} \qquad [13]$$

$$M^{tot.} = M_F^{eq.} + M_U^{eq.} + M_B^{eq.}$$

Optimization was carried out by minimizing the RSS differences according to

$$RSS = \sum_q \sum_{i=1}^{N} \left(I_q^{exp.}(t_i) - I_q^{calc.}(t_i, \zeta) \right)^2 \qquad [14]$$

where $I_q^{exp.}(t_i)$ and $I_q^{calc.}(t_i, \zeta)$ ($q \in$ {F, B, U, FU, UF, FB, BF, UB, BU}, ζ = {$cM^{tot.}$, k_{FU}, k_{UF}, k_{FB}, k_{BF}, k_{UB}, k_{BU}, R_F, R_U, R_B}) are the experimental and calculated NMR signal intensities at each mixing time t_i, and *N* is the total number of time points, subject to the constraint of the rates constants satisfying microscopic reversibility. Prior to fitting, signal losses from transverse ^{1}H relaxation during the pair of ^{13}C↔^{1}H magnetization transfer elements in the magnetization exchange pulse scheme were corrected by

multiplying each $I_q^{exp.}(t_i)$ by the appropriate factor, for example by $\exp(R_{2,\mathrm{F}}\tau)\times\exp(R_{2,\mathrm{U}}\tau)$ for $I_{FU}^{exp.}(t_i)$, where $R_{2,q}$ is the ^{1}H transverse relaxation rate of state q ($R_{2,\mathrm{F}}$ = 18.7 s^{-1}, $R_{2,\mathrm{U}}$ = 39.3 s^{-1}, and $R_{2,\mathrm{B}}$ = 109.9 s^{-1}) and τ is the magnetization transfer time (τ = 3.6 ms for each transfer period placed before and after the mixing time). ^{1}H transverse relaxation rates were measured as described previously (39). Minimization of the above target function was achieved using in-house written programs (Python 3.7), exploiting the Levenberg-Marquardt algorithm of the Lmfit python software package (https://lmfit.github.io/lmfit-py/). Distributions of fitted parameters were obtained by running 500 Monte-Carlo simulations, and fitted parameter errors were taken as the standard deviations of these parameter sets.

Supplementary Table

Supplementary Table 1 List of peptides identified in the LC-MS analyses

ID	Measured mass	Theoretical mass	Sequence (residue numbers annotated on top)
1	3134.62	3134.607	1 27 GMEAIAKHDFSATADDELSFRKTQILKI
2	3492.78	3492.774	1 30 GMEAIAKHDFSATADDELSFRKTQILKILNM
3	3247.7	3247.691	1 28 GMEAIAKHDFSATADDELSFRKTQILKIL
4	4553.06	4553.058	28 65 LNMEDDSNWYRAELDGKEGLIPSNYIEMKNHDGQYYFV
5	4194.9	4194.890	31 65 EDDSNWYRAELDGKEGLIPSNYIEMKNHDGQYYFV
6	4439.98	4439.974	29 65 NMEDDSNWYRAELDGKEGLIPSNYIEMKNHDGQYYFV

Supplementary Figures

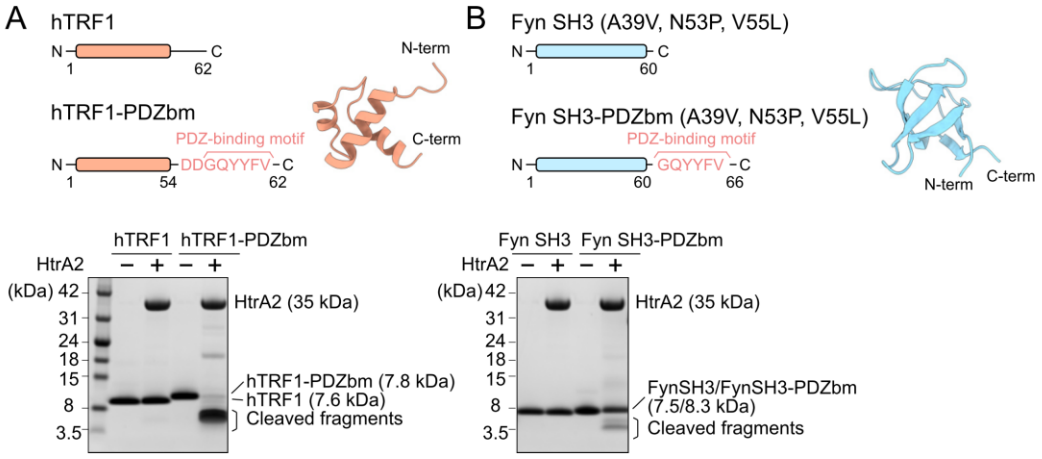

Figure S1. HtrA2 cleaves hTRF1-PDZbm and Fyn SH3-PDZbm but not hTRF1 and Fyn SH3. (A) (*left top*) Schematic representations of the hTRF1 constructs (hTRF1 and hTRF1-PDZbm) used in this study. (*right top*) NMR structure of hTRF1 (PDB ID: 1BA5) (40). (*bottom*) Gel-based proteolytic activity assays of wild-type HtrA2 using hTRF1 or hTRF1-PDZbm as substrates. (B) (*left top*) Schematic representations of a triple mutant (A39V, N53P, V55L) Fyn SH3 construct, without and with a C-terminal PDZ-binding motif (Fyn SH3 and Fyn SH3-PDZbm), as used in this study. (*right top*) NMR structure of the major conformer of the triple mutant Fyn SH3 domain (PDB ID: 2LP5) (12). (*bottom*) Gel-based proteolytic activity assays of wild-type HtrA2 with Fyn SH3 or Fyn SH3-PDZbm as substrates. In the gel-based proteolytic assays, 50 μM substrate proteins were incubated with or without 10 μM HtrA2 (monomer concentration) at 37 °C for two hours, and the reaction mixture was subjected to SDS-PAGE analyses. The assignment of each band is shown to the right.

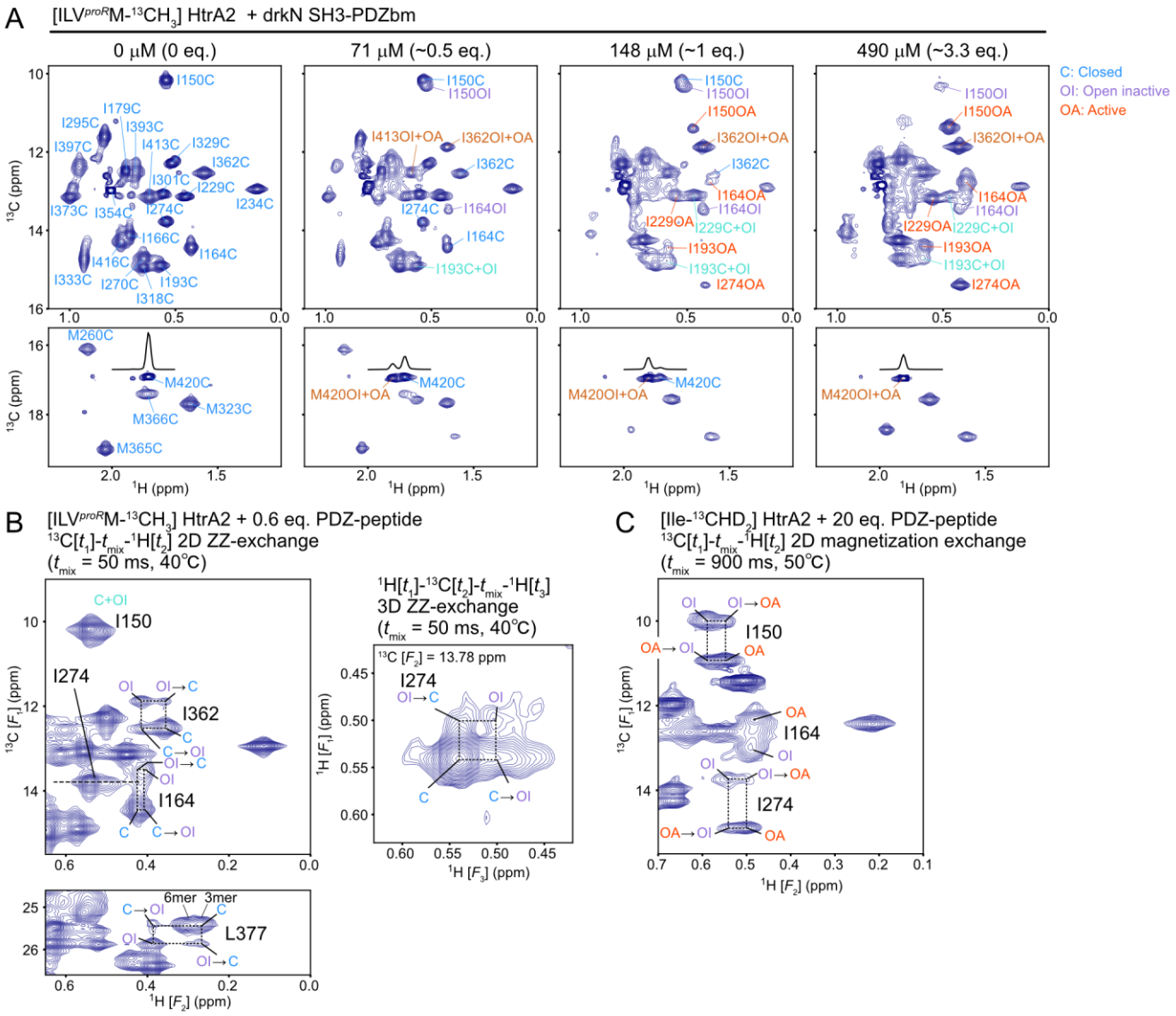

Figure S2. Titration of drkN SH3-PDZbm and assignments of methyl signals of HtrA2. (A) ^{13}C-^{1}H HMQC spectra of 150 μM (monomer concentration) U-^{2}H, *proR* ILVM I441V/S306A HtrA2 with 0, 71, 148, and 490 μM added U-^{2}H,^{15}N drkN SH3-PDZbm. The assignments of the signals from each state are indicated with color as follows, C: blue, OI: purple, OA: red, C+OI: turquoise, and OI+OA: brown. The spectra are as per Figure 2B of the main text, but with larger chemical shift regions plotted. (B) (*left*) Correlation maps of ^{13}C[t_1]-t_{mix}-^{1}H[t_2] 2D ZZ-exchange and (*right*) ^{1}H[t_1]-^{13}C[t_2]-t_{mix}-^{1}H[t_3] 3D ZZ-exchange spectra correlating C and OI states. The spectra were recorded at a static magnetic field strength of 23.5 Tesla and 40 °C, using a 160 μM (monomer concentration) U-^{2}H, *proR* ILVM S306A HtrA2 sample

with 100 μM ^{2}H-labeled PDZ peptide in an NMR buffer consisting of 20 mM HEPES-NaOH (pD 7.4), 1 mM EDTA, 100% D_2O, as described previously (1). A mixing time of 50 ms was used. For L377, two signals corresponding to the 6mer and 3mer in the C state are observed. (C) Ile region of a $^{13}C[t_1]$-t_{mix}-$^{1}H[t_2]$ 2D ^{13}C magnetization exchange spectrum correlating the OI and OA states. The spectrum was measured at a static magnetic field strength of 14.0 Tesla and 50 °C, using a 200 μM (monomer concentration) U-^{2}H, Ile-$^{13}CHD_2$ S306A/I441V sample containing 4 mM PDZ-peptide in an NMR buffer consisting of 20 mM HEPES-NaOH (pD 7.4), 1 mM EDTA, 100% D_2O, as described previously (2). A mixing time of 900 ms was used.

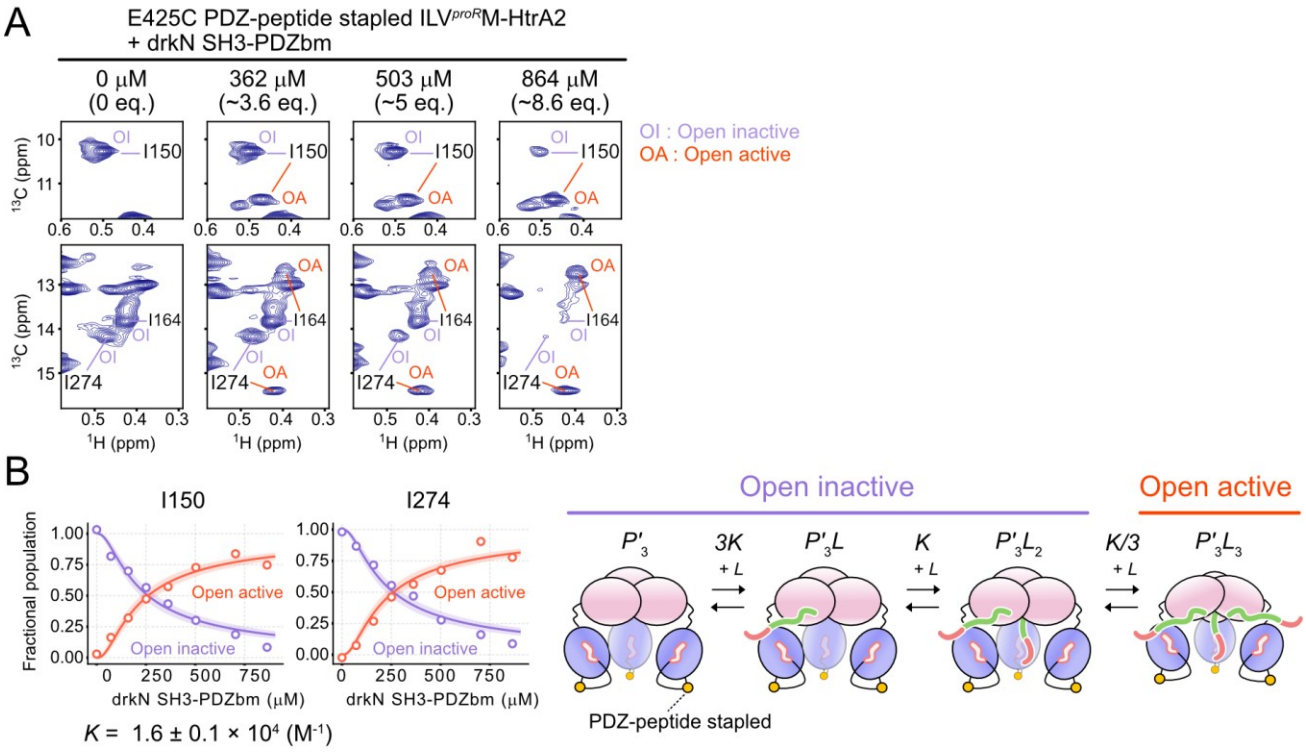

Figure S3. Titration of drkN SH3-PDZbm into a solution of PDZ peptide-stapled HtrA2 to measure K_3. (A) ^{13}C-^{1}H HMQC correlation maps of 100 μM U-^{2}H, *proR* ILVM E425C/S306A/I441V PDZ peptide-stapled HtrA2 in the presence of various concentrations of U-^{2}H,^{15}N drkN SH3-PDZbm, as shown. The spectra were recorded at 40 °C and 18.8 Tesla. The assignments for the OI and OA state signals of I150, I164, and I274 are indicated. (B) (*left*) Plots of the fractional populations of the OI (purple) and OA (red) states calculated from the I150 and I274 correlations as a function of the concentration of drkN SH3-PDZbm. The solid lines are the fitted curves and the 95% CI of each fitted curve is contained within the thick line estimated from Monte Carlo error analyses (41). The best-fit value and the estimated error of the microscopic association constant *K* are shown below. The thermodynamic model along with cartoon representations of each state used in the fits of the titration data are shown to the right.

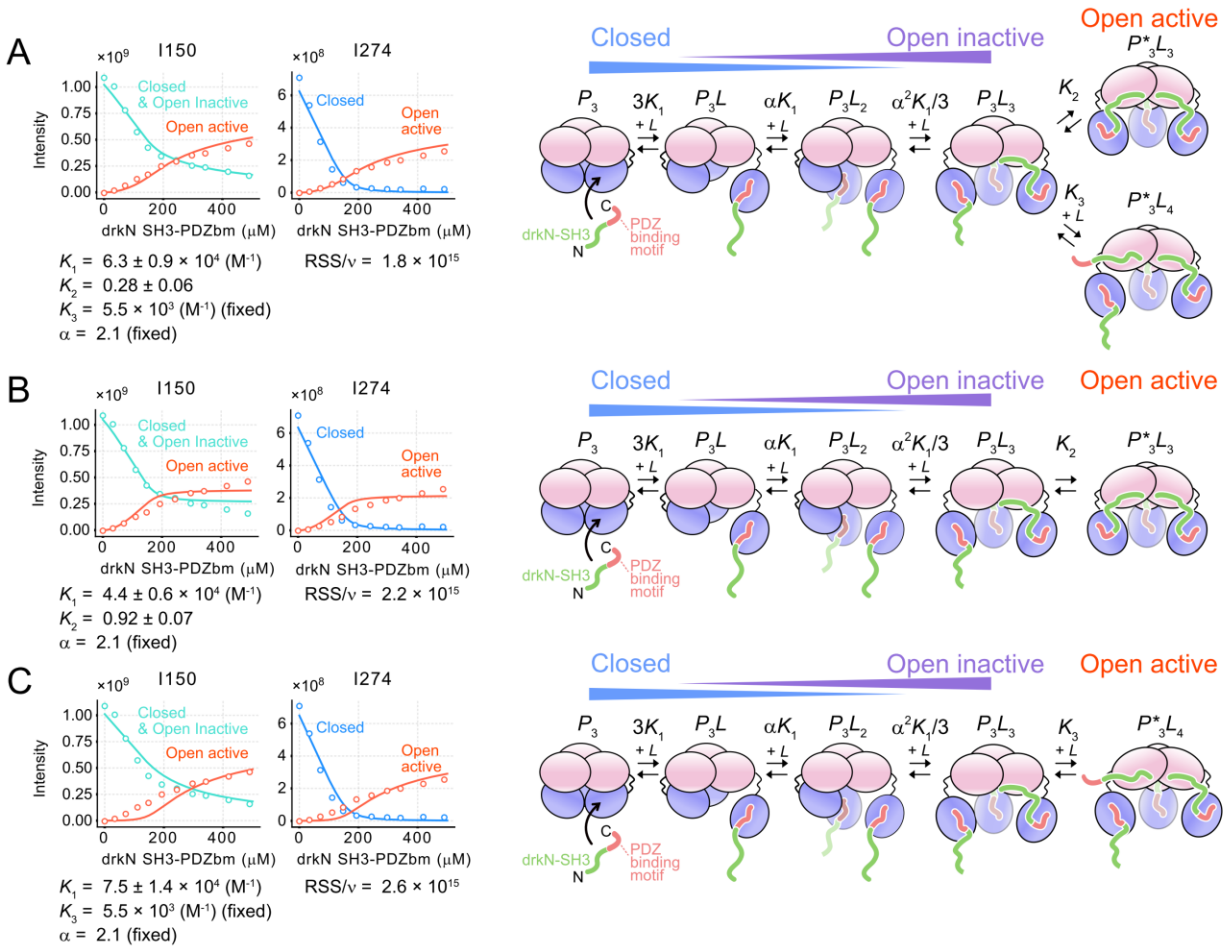

Figure S4. The branched pathway model of Figure 2D best fits titration profiles of drkN SH3-PDZbm. Titration profiles quantifying the binding of drkN SH3-PDZbm to U-^{2}H, *proR* ILVM-$^{13}CH_3$ S306A/I441V HtrA2 were fit to different models. In panel (A), the best fit model, Figure 2D, is shown as a reference. In the model shown in (B) the $P^*_3L_4$ state is eliminated, while in the model shown in (C) $P^*_3L_3$ is not included. (*left*) Plots of the intensities of methyl correlations of I150 and I274 as a function of the concentration of drkN SH3-PDZbm. The solid lines are the fitted curves. The signal intensities of the C, OA, and C+OI states are colored blue, red, and turquoise, respectively. The fractional populations of the C, OI, and OA states (p_C, p_{OI}, and p_{OA}) were calculated using $p_C = (3[P_3]+2[P_3L]+[P_3L_2])/C_T$, $p_{OI} = ([P_3L]+2[P_3L_2]+3[P_3L_3])/C_T$, $p_{OA} = (3[P^*_3L_3]+ 3[P^*_3L_4])/C_T$. In all models, K_3 (= 5,470 M^{-1}) and α (= 2.1) were fixed. The fitted parameters and RSS/ν (ν = the number of the data points - the number of variables) are shown below the plots. (*right*) The thermodynamic models along with cartoon representations of each state used in the fits are displayed.

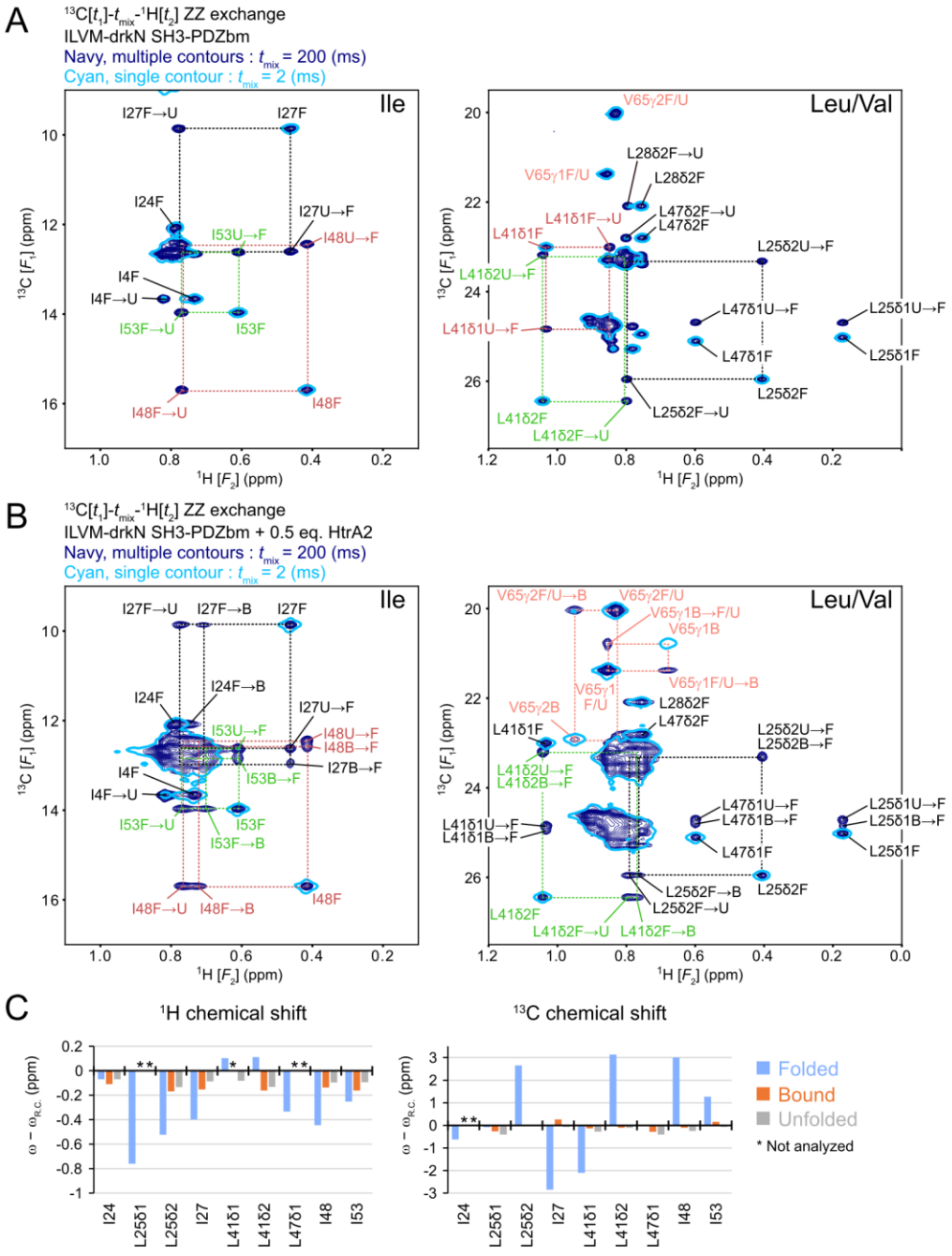

Figure S5. Assignment of the U, F, and B states of drkN SH3-PDZbm by ZZ-exchange. (A, B) ^{13}C[t_1]-t_{mix}-^{1}H[t_2] 2D ZZ-exchange spectra of 150 μM U-^{2}H, ILVM drkN SH3-PDZbm in the absence (A) and in the presence (B) of 75 μM (monomer concentration) U-^{2}H, S306A/I441V HtrA2. The spectra obtained

with t_{mix} of 2 ms (cyan single contour, diagonal peaks only) and 200 ms (navy multiple contours, both diagonal and exchange cross-peaks) are overlaid to highlight the diagonal- and exchange cross-peaks. The spectra were recorded at a static magnetic field strength of 23.5 Tesla and 40 °C in an NMR buffer consisting of 20 mM HEPES-NaOH (pD 7.4), 50 mM NaCl, 1 mM EDTA, 100% D_2O. The diagonal- and exchange cross-peaks are connected by dotted lines for each residue (black, green, pink, and dark-red). (C) Plots of differences between ^{1}H (*left*)/^{13}C (*right*) chemical shifts of the F (blue), B (orange), and U (gray) states of drkN SH3-PDZbm and random coil values (42). The residues that were not analyzed due to overlapping signals are indicated with an asterisk.

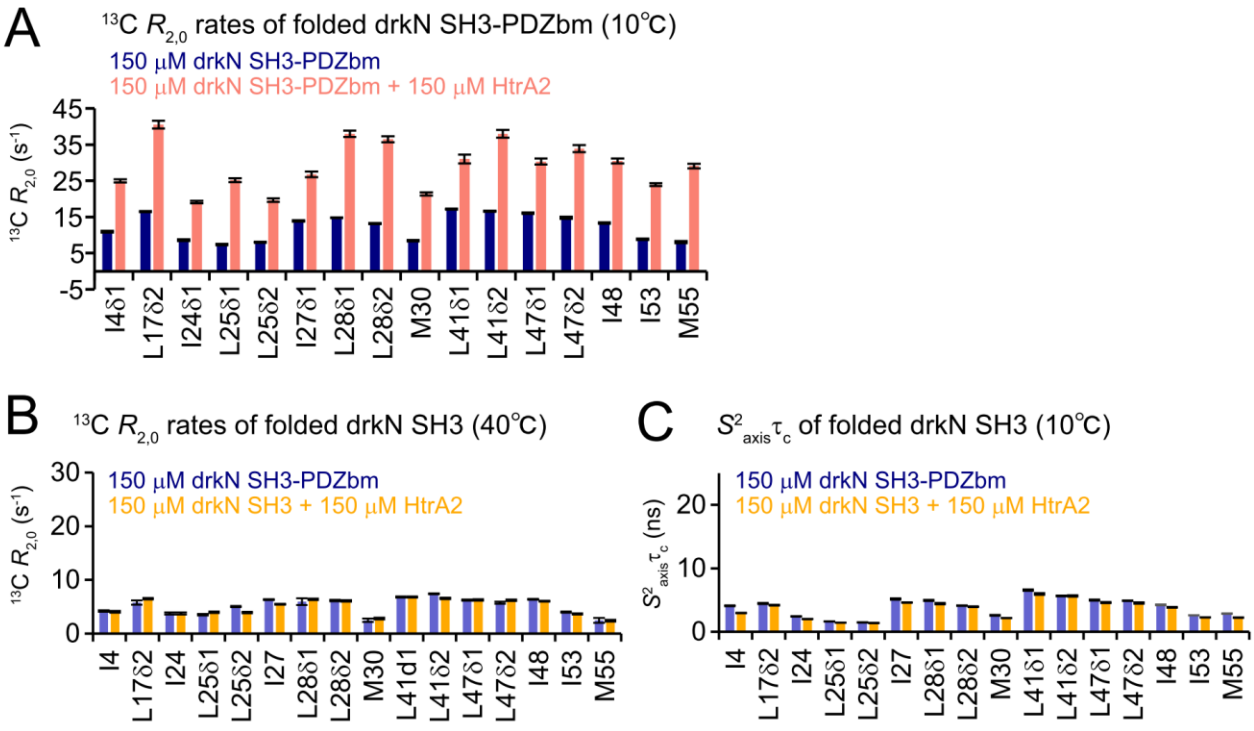

Figure S6. drkN SH3 ^{13}C transverse relaxation rates and order parameters. (A) Plots of ^{13}C single quantum transverse relaxation rates of $^{13}CH_3$ methyl groups of U-^{2}H, ILVM drkN SH3-PDZbm measured with a 2 kHz CPMG field, with (pink) and without (navy) U-^{2}H, S306A/I441V HtrA2. The measurements were performed at 10 °C and 23.5 Tesla. (B) Plots of ^{13}C single quantum transverse relaxation rates of U-^{2}H, ILVM drkN SH3-PDZbm (navy) and U-^{2}H, ILVM drkN SH3 (without PDZ-binding motif) in the presence of U-^{2}H, S306A/I441V HtrA2 (orange) measured using a 2 kHz CPMG field. The measurements were performed at 40 °C and 23.5 Tesla. (C) Comparison of the order parameter squared multiplied by the rotational correlation time ($S^2_{axis}\tau_c$) of methyl 3-fold symmetry axes of U-^{2}H, ILVM drkN SH3-PDZbm (navy) and U-^{2}H, ILVM drkN SH3 with U-^{2}H, S306A/I441V HtrA2 (orange). The measurements were performed at 10 °C and 23.5 Tesla.

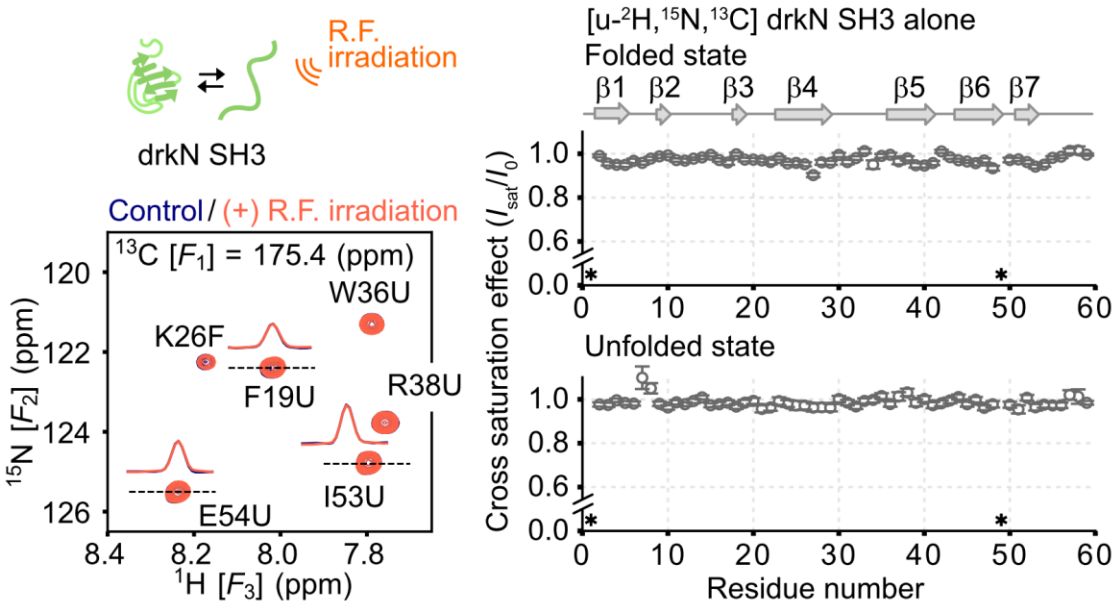

Figure S7. TCS control experiment. (*left top*) Schematic representation of the control TCS experiment to evaluate whether saturation of residual protons (< 2%) in a U-^{2}H drkN SH3 sample leads to measurable attenuation of amide signals. (*left bottom*) ^{15}N-^{1}H slices from 3D TROSY-HNCO spectra of U-^{2}H, ^{15}N, ^{13}C drkN SH3 with (orange) and without (navy) ^{1}H irradiation of the aliphatic region. 1D cross-sections for F19U, I53U, and E54U are shown. (*right*) Plots of cross-saturation effects in the folded and unfolded states of drkN SH3. These were calculated from the intensity ratios obtained by comparing corresponding cross-peaks in a pair of datasets obtained with and without ^{1}H radio frequency (R.F.) irradiation. The measurement was performed at 10 °C and 14.0 Tesla. Asterisks denote P49 or residues that could not be analyzed due to peak broadening.

SI References

1. Y. Toyama, R. W. Harkness, T. Y. T. Lee, J. T. Maynes, L. E. Kay, Oligomeric assembly regulating mitochondrial HtrA2 function as examined by methyl-TROSY NMR. *Proc. Natl. Acad. Sci. USA* **118**, e2025022118 (2021).

2. Y. Toyama, R. W. Harkness, L. E. Kay, Dissecting the role of interprotomer cooperativity in the activation of oligomeric high-temperature requirement A2 protein. *Proc. Natl. Acad. Sci. USA* **118**, e2111257118 (2021).

3. V. Tugarinov, V. Kanelis, L. E. Kay, Isotope labeling strategies for the study of high-molecular-weight proteins by solution NMR spectroscopy. *Nat. Protoc.* **1**, 749–754 (2006).

4. P. Gans, *et al.*, Stereospecific Isotopic Labeling of Methyl Groups for NMR Spectroscopic Studies of High-Molecular-Weight Proteins. *Angew. Chem. Int. Ed.* **49**, 1958–1962 (2010).

5. A. Sekhar, *et al.*, Conserved conformational selection mechanism of Hsp70 chaperone-substrate interactions. *eLife* **7** (2018).

6. Y. Tao, S. V Strelkov, V. V Mesyanzhinov, M. G. Rossmann, Structure of bacteriophage T4 fibritin: a segmented coiled coil and the role of the C-terminal domain. *Structure* **5**, 789–798 (1997).

7. S. Frank, *et al.*, Stabilization of short collagen-like triple helices by protein engineering. *J. Mol. Biol.* **308**, 1081–1089 (2001).

8. X. Yang, *et al.*, Highly stable trimers formed by human immunodeficiency virus type 1 envelope glycoproteins fused with the trimeric motif of T4 bacteriophage fibritin. *J. Virol.* **76**, 4634–42

(2002).

9. S. Meier, S. Güthe, T. Kiefhaber, S. Grzesiek, Foldon, The Natural Trimerization Domain of T4 Fibritin, Dissociates into a Monomeric A-state Form containing a Stable β-Hairpin: Atomic Details of Trimer Dissociation and Local β-Hairpin Stability from Residual Dipolar Couplings. *J. Mol. Biol.* **344**, 1051–1069 (2004).

10. D. M. Korzhnev, *et al.*, Low-populated folding intermediates of Fyn-SH3 characterized by relaxation dispersion NMR. *Nature* **430**, 586–590 (2004).

11. P. Neudecker, *et al.*, Identification of a Collapsed Intermediate with Non-native Long-range Interactions on the Folding Pathway of a Pair of Fyn SH3 Domain Mutants by NMR Relaxation Dispersion Spectroscopy. *J. Mol. Biol.* **363**, 958–976 (2006).

12. P. Neudecker, *et al.*, Structure of an Intermediate State in Protein Folding and Aggregation. *Science* **336**, 362–366 (2012).

13. A. Sekhar, R. Rosenzweig, G. Bouvignies, L. E. Kay, Mapping the conformation of a client protein through the Hsp70 functional cycle. *Proc. Natl. Acad. Sci. USA* **112**, 10395–10400 (2015).

14. R. Rosenzweig, A. Sekhar, J. Nagesh, L. E. Kay, Promiscuous binding by Hsp70 results in conformational heterogeneity and fuzzy chaperone-substrate ensembles. *eLife* **6** (2017).

15. T. L. Religa, A. M. Ruschak, R. Rosenzweig, L. E. Kay, Site-directed methyl group labeling as an NMR probe of structure and dynamics in supramolecular protein systems: Applications to the proteasome and to the ClpP protease. *J. Am. Chem. Soc.* **133**, 9063–9068 (2011).

16. R. Huang, *et al.*, Unfolding the mechanism of the AAA+ unfoldase VAT by a combined cryo-EM, solution NMR study. *Proc. Natl. Acad. Sci. USA*, E4190–E4199 (2016).

17. C. A. Schneider, W. S. Rasband, K. W. Eliceiri, NIH Image to ImageJ: 25 years of image analysis. *Nat. Methods* **9**, 671–675 (2012).

18. A. Gattiker, W. V Bienvenut, A. Bairoch, E. Gasteiger, FindPept, a tool to identify unmatched masses in peptide mass fingerprinting protein identification. *Proteomics* **2**, 1435–44 (2002).

19. F. Delaglio, *et al.*, NMRPipe: A multidimensional spectral processing system based on UNIX pipes. *J. Biomol. NMR* **6**, 277–293 (1995).

20. J. J. Helmus, C. P. Jaroniec, Nmrglue: an open source Python package for the analysis of multidimensional NMR data. *J. Biomol. NMR* **55**, 355–367 (2013).

21. S. G. Hyberts, K. Takeuchi, G. Wagner, Poisson-gap sampling and forward maximum entropy reconstruction for enhancing the resolution and sensitivity of protein NMR data. *J. Am. Chem. Soc.* **132**, 2145–2147 (2010).

22. J. Ying, F. Delaglio, D. A. Torchia, A. Bax, Sparse multidimensional iterative lineshape-enhanced (SMILE) reconstruction of both non-uniformly sampled and conventional NMR data. *J. Biomol. NMR* **68**, 101–118 (2017).

23. A. Ahlner, M. Carlsson, B.-H. Jonsson, P. Lundström, PINT: a software for integration of peak volumes and extraction of relaxation rates. *J. Biomol. NMR* **56**, 191–202 (2013).

24. M. Niklasson, *et al.*, Comprehensive analysis of NMR data using advanced line shape fitting. *J. Biomol. NMR* **69**, 93–99 (2017).

25. A. Mittermaier, L. E. Kay, Measurement of Methyl ^{2}H Quadrupolar Couplings in Oriented Proteins. How Uniform Is the Quadrupolar Coupling Constant? *J. Am. Chem. Soc.* **121**, 10608–10613 (1999).

26. V. Tugarinov, P. M. Hwang, J. E. Ollerenshaw, L. E. Kay, Cross-correlated relaxation enhanced ^{1}H-^{13}C NMR spectroscopy of methyl groups in very high molecular weight proteins and protein complexes. *J. Am. Chem. Soc.* **125**, 10420–8 (2003).

27. L. E. Kay, Artifacts can emerge in spectra recorded with even the simplest of pulse schemes: an HMQC case study. *J. Biomol. NMR* **73**, 423–427 (2019).

28. P. Lundström, P. Vallurupalli, T. L. Religa, F. W. Dahlquist, L. E. Kay, A single-quantum methyl ^{13}C-relaxation dispersion experiment with improved sensitivity. *J. Biomol. NMR* **38**, 79–88 (2007).

29. H. Sun, L. E. Kay, V. Tugarinov, An optimized relaxation-based coherence transfer NMR experiment for the measurement of side-chain order in methyl-protonated, highly deuterated proteins. *J. Phys. Chem. B* **115**, 14878–14884 (2011).

30. T. L. Religa, R. Sprangers, L. E. Kay, Dynamic regulation of archaeal proteasome gate opening as studied by TROSY NMR. *Science* **328**, 98–102 (2010).

31. C. Griesinger, M. Sattler, Heteronuclear multidimensional NMR experiments for the structure determination of proteins in solution employing pulsed field gradients. *Prog. Nucl. Magn. Reson. Spectrosc.* **34**, 93–158 (1999).

32. S. C. Panchal, N. S. Bhavesh, R. V. Hosur, Improved 3D triple resonance experiments, HNN and

HN(C)N, for H^N and ^{15}N sequential correlations in (^{13}C, ^{15}N) labeled proteins: application to unfolded proteins. *J. Biomol. NMR* **20**, 135–47 (2001).

33. H. Takahashi, T. Nakanishi, K. Kami, Y. Arata, I. Shimada, A novel NMR method for determining the interfaces of large protein-protein complexes. *Nat. Struct. Biol.* **7**, 220–3 (2000).

34. T. Nakanishi, *et al.*, Determination of the Interface of a Large Protein Complex by Transferred Cross-saturation Measurements. *J. Mol. Biol.* **318**, 245–249 (2002).

35. T. Ueda, *et al.*, Cross-saturation and transferred cross-saturation experiments. *Q. Rev. Biophys.* **47**, 143–187 (2014).

36. D. Yang, L. E. Kay, Improved ^{1}HN-detected triple resonance TROSY-based experiments. *J. Biomol. NMR* **13**, 3–10 (1999).

37. D. Nietlispach, Suppression of anti-TROSY lines in a sensitivity enhanced gradient selection TROSY scheme. *J. Biomol. NMR* **31**, 161–166 (2005).

38. E. Kupce, G. Wagner, Ē. Kupče, G. Wagner, Wideband Homonuclear Decoupling in Protein Spectra. *J. Magn. Reson.* **109**, 329–333 (1995).

39. M. P. Latham, A. Sekhar, L. E. Kay, Understanding the mechanism of proteasome 20S core particle gating. *Proc. Natl. Acad. Sci. USA* **111**, 5532–5537 (2014).

40. T. Nishikawa, A. Nagadoi, S. Yoshimura, S. Aimoto, Y. Nishimura, Solution structure of the DNA-binding domain of human telomeric protein, hTRF1. *Structure* **6**, 1057–1065 (1998).

41. W. H. Press, B. P. Flannery, S. A. Teukolsky, W. T. Vetterling, Numerical Recipes in C. The Art of Scientific Computing 2nd edn (Cambridge Univ. Press, 1992).

42. D. S. Wishart, C. G. Bigam, A. Holm, R. S. Hodges, B. D. Sykes, ^{1}H, ^{13}C and ^{15}N random coil NMR chemical shifts of the common amino acids. I. Investigations of nearest-neighbor effects. *J. Biomol. NMR* **5**, 67–81 (1995).